Generalized scaling laws for the irrotational motions bordering a turbulent region

Generalized scaling laws for the irrotational motions bordering a turbulent region

Marco Zecchetto,[1] Ricardo P. Xavier,[1] Miguel A. C. Teixeira,[2] and Carlos B. da Silva[1]
[1]*IDMEC/LAETA, Instituto Superior Técnico, Universidade de Lisboa, 1049-001 Lisboa, Portugal*
[2]*Department of Meteorology, University of Reading, Meteorology Building, Whiteknights Road, Earley Gate, Reading RG6 6ET, United Kingdom*

(Received 6 November 2023; accepted 17 May 2024; published 17 June 2024)

In turbulent free shear flows such as jets and wakes, and also in turbulent boundary layers, the turbulent region is bounded by a region of irrotational flow where the magnitude of the potential velocity fluctuations can be very high. This is particularly true close to the turbulent-nonturbulent interface layer (TNTI) that separates the regions of turbulent (rotational) and nonturbulent (irrotational) fluid motion in these flows. Previous works have shown that for distances from the TNTI x_2 much bigger than the integral scale L in the nearby turbulent region ($x_2 \gg L$), the variance of the velocity fluctuations $\langle u_i^2 \rangle$ ($i = 1, 2, 3$) depends on the shape of the kinetic energy spectrum in the infrared region $E(k) \sim k^n$ [O. M. Phillips, Proc. Camb. Phil. Soc. **51**, 220 (1955); Xavier *et al.*, J. Fluid Mech. **918**, A3 (2021)]. Using rapid distortion theory, we derive the generalized scaling laws for the potential velocity fluctuations, at distances sufficiently far from the TNTI layer, for any value of n. While the cases $n = 4$ (Batchelor turbulence) and $n = 2$ (Saffman turbulence) have been previously derived, with $\langle u_i^2 \rangle \sim x_2^{-4}$ and $\langle u_i^2 \rangle \sim x_2^{-3}$, for $n = 4$ and $n = 2$, respectively [O. M. Phillips, Proc. Camb. Phil. Soc. **51**, 220 (1955); Xavier *et al.*, J. Fluid Mech. **918**, A3 (2021).], we extend these results by including any other value of n. In particular, we obtain $\langle u_i^2 \rangle \sim x_2^{-2}$ and $\langle u_i^2 \rangle \sim x_2^{-4}$, for $n = 1$ and $n \geqslant 5$, respectively, while $n = 3$ yields $\langle u_i^2 \rangle \sim x_2^{-4} \ln(x_2)$. These theoretical results are confirmed by direct numerical simulations of turbulent fronts evolving into an irrotational flow region in the absence of mean shear.

DOI: 10.1103/PhysRevE.109.065107

I. INTRODUCTION

Regions of irrotational or nonturbulent flow exist in virtually all canonical free shear flows, e.g., jets, wakes, and mixing layers, and are also found adjacent to turbulent boundary layers [1]. An abrupt transition exists in these flows between the nonturbulent (NT) and turbulent (T) flow regions that are separated by the so-called turbulent-nonturbulent interface layer (TNTI), which is highly contorted by the large range of existing scales in the turbulent region [2–4]. The importance of this layer is motivated by the mechanism of turbulent entrainment whereby fluid initially pertaining to the nonturbulent region is drawn into the turbulent region across this interface and becomes part of the turbulent region.

An interesting and often neglected fact about the flow field in the irrotational region consists of the existence of potential velocity fluctuations caused by the presence of the eddy structures in the T region [5–7], and naturally the magnitude of these fluctuations tends to increase when approaching the turbulent region. Whereas the vorticity displays an abrupt change across the TNTI layer [8], the velocity fluctuations evolve smoothly as shown in Ref. [9]. However, while the cross Reynolds stresses, $\langle u_i u_j \rangle$, with $i \neq j$, are rigorously zero in the NT flow region [10] the normal Reynolds stresses, $\langle u_i u_j \rangle$ with $i = j$, are very high in the NT region near the T region. For example, Refs. [3,9] have shown that the streamwise normal Reynolds stresses in the TNTI layer from a planar turbulent jet are about one-half their value inside the turbulent core region of the flow.

To investigate the velocity fluctuations in the NT region near the boundary of a T region, we define the three spatial coordinates and the time, $\vec{x} = x_i$ ($i = 1, 2, 3$) and t, respectively, where the index $i = 2$ corresponds to the direction normal to the TNTI layer. The Reynolds decomposition is used to separate the total velocity field $U_i(\vec{x})$ into the sum its mean $\langle U_i(\vec{x}) \rangle$ and fluctuating velocity components $u_i(\vec{x}, t)$, i.e., $\langle U_i(\vec{x}) \rangle + u_i(\vec{x}, t)$, and the brackets "$\langle\rangle$" represent an averaging operation (described later).

Phillips [10] pioneered the investigation of the potential velocity fluctuations in the NT region by providing analytical descriptions for the evolution of the second-order moments of the fluctuating velocity components $\langle u_i u_j(x_2) \rangle$ ($i, j = 1, 2, 3$), as a function of the distance from the T region layer, x_2, for distances much bigger than the integral scale of turbulence, $x_2 \gg L$. By assuming that the kinetic energy spectrum has an infrared (low wave number) region in the form $E(k) \sim k^4$, where k is the wave number (representing a Batchelor spectrum [11]), Phillips [10] obtained the following scaling laws for the variation of the velocity fluctuations: $\langle u_i^2(x_2) \rangle \sim x_2^{-4}$ ($i, j = 1, 2, 3$), and $\langle u_i u_j(x_2) \rangle = 0$ for $i \neq j$. Carruthers and Hunt [12] used rapid distortion theory (RDT) to extend the results derived by Ref. [10] for all the range of coordinates x_2 for NT regions in stable stratification, and in the absence of mean shear (for a review on RDT, see Ref. [13]). For coordinates $x_2 \gg L$ and in the absence of stratification, the asymptotic relations $\langle u_i^2(x_2) \rangle \sim x_2^{-4}$ ($i, j = 1, 2, 3$) are recovered. Teixeira and da Silva [14] later extended these results by considering the effects of a thin viscous layer roughly coinciding with the

TNTI layer. As in Ref. [12], RDT allowed them to obtain the full profiles of all important turbulence quantities as a function of the distance from the TNTI, x_2, but again, when analyzing large distances $x_2 \gg L$, the scaling relations $\langle u_i^2(x_2)\rangle \sim x_2^{-4}$ $(i, j = 1, 2, 3)$ were recovered.

The asymptotic relations described above for the potential velocity fluctuations in the NT region have been observed in several experimental works, such as in turbulent wakes [15–17], turbulent mixing layers [18], turbulent jets [19,20], and turbulent boundary layers [21,22]. The numerical works reporting these asymptotic relations include the direct numerical simulations (DNSs) of turbulent planar jets [9], and shear-free turbulent fronts (turbulent fronts evolving into a region of NT flow in the absence of mean shear) [14].

It is important to recall that all the above results were derived assuming the turbulent flow in the nearby T region is described by a *Batchelor spectrum* [11], where $E(k) \sim k^4$ (for $k \ll 1/L$). However, it is well-known that spectra of the form $E(k) \sim k^2$ [23], also denoted as the Saffman spectrum [11], do exist in many turbulent flows, and several authors also mention spectra with the general form $E(k) \sim k^n$, where n is a constant, different from $n = 4$ (Batchelor spectrum) or $n = 2$ (Saffman spectrum) [24–27]. Indeed, it is well-known that the shape of the kinetic energy spectrum in the infrared region $E(k) \sim k^n$ determines the evolution of the main turbulence quantities in decaying isotropic turbulence (see Refs. [11,13] for an exhaustive description of the several isotropic decay theories). Besides the above-mentioned cases of $E(k) \sim k^2$ (Saffman spectrum) and $E(k) \sim k^4$ (Batchelor spectrum), a decay solution with a constant integral scale (e.g., as when the integral scale reaches the domain size) corresponds to $E(k) \sim k^\infty$, whereas $E(k) \sim k$ represents a decay with constant Reynolds number [27]. Vassilicos [26] has shown that at least for $n \geqslant 2$, virtually all cases are physically consistent.

Using RDT and by assuming that the T region behaves as Saffman turbulence (Xavier *et al.* [28]) were able to obtain the asymptotic laws governing the turbulence quantities neighboring the NT region. Specifically, they showed that for NT regions near a T region with $E(k) \sim k^2$ (for $k \ll 1/L$) the velocity variance decreases, as a function of the distance from the TNTI (x_2), as $\langle u_i^2\rangle \sim x_2^{-3}$ $(i = 1, 2, 3)$, while the Taylor microscale λ, and viscous dissipation rate ε vary as $\langle\lambda\rangle \sim x_2$ and $\langle\varepsilon\rangle \sim x_2^{-5}$, respectively. These results were confirmed by DNS of shear free turbulence (SFT).

It is important to recall that in the above-mentioned work, it was shown that the RDT results for the asymptotic behavior of the potential velocity fluctuations in the NT region are independent of the value of the Reynolds number of the flow and also of the peak of the kinetic energy spectrum, which is related to the integral scale of the turbulence in the nearby T region. Also, the fact that these asymptotic laws (including the case for $E(k) \sim k^2$) have been observed in several different flow configurations such as in turbulent jets, turbulent wakes, and turbulent boundary layers suggests that the presence or absence of mean shear is not important for these laws, which should be valid in any other NT flow region (provided $x_2 \gg L$).

In the present paper, and using RDT, we extend the results described above for T regions exhibiting a general energy spectrum, i.e., with an infrared region defined by $E(k) \sim k^n$, where n is an integer constant, for $k \ll 1/L$. The asymptotic laws for the variance of the potential velocity fluctuations extend the results previously obtained by Refs. [10,28] for kinetic energy spectra with any value of the integer constant n. The results reduce to the previous solutions of $\langle u_i^2\rangle \sim x_2^{-4}$ and $\langle u_i^2\rangle \sim x_2^{-3}$, corresponding to $n = 4$ (Batchelor turbulence) and $n = 2$ (Saffman turbulence), respectively, and provide solutions for other values of n. In particular, we obtain $\langle u_i^2\rangle \sim x_2^{-2}$ and $\langle u_i^2\rangle \sim x_2^{-4}$ for $n = 1$ and $n \geqslant 5$, respectively, while the case $n = 3$ leads to $\langle u_i^2\rangle \sim x_2^{-4}\ln(x_2)$. The theoretical results are confirmed by DNS of shear-free turbulence.

This paper is organized as follows. The next section (Sec. II) extends the analytical results obtained by Xavier *et al.* [28] using RDT by considering an infrared kinetic energy spectrum with a form $E(k) \sim k^n$, for any integer value of n. Section III describes the numerical methods, simulations, and validation of the simulations used in the present paper, and assesses the theoretical results using DNS. The paper ends with an overview of the main results and Conclusions (Sec. IV).

II. THEORY FOR VELOCITY FLUCTUATIONS IN AN IRROTATIONAL FLOW REGION

In a recent paper, Xavier *et al.* [28] extended the results of Phillips [10] regarding the decay of the velocity fluctuations in an irrotational flow region adjacent to a homogeneous and isotropic turbulence region as one moves away from the TNTI. They found that when a Saffman energy spectrum with a variation at low wave numbers $E(k) \sim k^2$ is adopted to describe the turbulence, the velocity variances in the irrotational flow region decay as $\langle u_i^2\rangle \sim x_2^{-3}$ (x_2 is the distance from the TNTI). This is in contrast with Phillips's [10] original finding, rediscovered using RDT by Teixeira and da Silva [14], assuming a Batchelor spectrum that varies as $E(k) \sim k^4$ at low wave numbers, which states that the velocity variances vary as $\langle u_i^2\rangle \sim x_2^{-4}$.

These results are intriguing, as a pattern between them is not obvious, so they will be extended here to an energy spectrum of the turbulence that varies at low wave numbers as $E(k) \sim k^n$. The corresponding form of the decay of the velocity variances with x_2 will be derived theoretically. A firmer connection between the results of Xavier *et al.* [28] and the previous results of Phillips [10] will also be established by relating the different approaches used by these authors via specification of the spectrum forcing the velocity fluctuations. Finally, we will substantiate and justify the result, advanced by all these previous authors without formal justification, that the qualitative asymptotic behavior of the velocity variances does not depend on the high-wave-number range of the assumed turbulence energy spectrum.

As in Teixeira and da Silva [14] and Xavier *et al.* [28], RDT is adopted here. This approach is more specific than the one used by Phillips [10], where the forcing of the irrotational velocity fluctuations is simply specified at the TNTI. It will be shown that the RDT approach is a particular case of Phillips's approach, which allows one to be more systematic regarding the characterization of the turbulence generating the irrotational velocity fluctuations. These two approaches were

shown by Teixeira and da Silva [14] to give the same type of decay rate of the velocity variances for the particular case of a Batchelor energy spectrum.

The variety of RDT used in this paper accounts for the effect of a suddenly inserted boundary (in the present case, a turbulent-nonturbulent interface). This approach goes back to the treatment of shear-free turbulence near a solid wall by Hunt and Graham [29], and of an interface between unstratified turbulence and a stably stratified nonturbulent flow region by Carruthers and Hunt [12]. In this approach, we add irrotational velocity corrections to the homogeneous turbulent velocity field to satisfy the boundary conditions at the relevant boundary (zero normal velocity in the case of the wall considered by Hunt and Graham [29], and continuity of the normal velocity and pressure in the case of the turbulent-nonturbulent interface of Carruthers and Hunt [12]. This approach has been used subsequently to treat in more detail the characteristics of turbulence at a turbulent-nonturbulent interface by Teixeira and da Silva [14], and Xavier *et al.* [28], the latter of which the present paper extends. As shown both in Xavier *et al.* [28] and in the present paper (see below), this approach predicts the decay of velocity variances in the nonturbulent part of the flow to be $\propto x_2^{-4}$ for a von Karman energy spectrum (with a low wave-number range $\propto k^4$. Although its performance in previous studies partly justifies this approach, in practice, the sudden insertion of a turbulent-nonturbulent interface is approximately realized when a turbulent jet or plume exits a pipe (although, in that case, the turbulence is previously bounded by a solid boundary).

In Phillips [10], the irrotational velocity fluctuations are driven by the 2D spectrum $\theta(k_1, k_3)$ of the velocity fluctuations perpendicular to the TNTI, u_2, at the TNTI, i.e., $x_2 = 0$. According to Eq. (19) of Phillips [10] or Eq. (2.2) of Xavier *et al.* [28], this spectrum is defined as

$$\theta(k_1,k_3) = \frac{1}{(2\pi)^2}\int_{-\infty}^{+\infty}\int_{-\infty}^{+\infty}\langle u_2(x_1,x_2=0,x_3) \times u_2(x_1+r_1,x_2=0,x_3+r_3)\rangle e^{-i(k_1x_1+k_3x_3)}dr_1dr_3, \tag{1}$$

where (x_1, x_2, x_3) is the spatial position, $(r_1, 0, r_2)$ is the spatial lag along a plane parallel to the TNTI, and $(k_1, 0, k_3)$ is the wave-number vector parallel to the TNTI.

The velocity fluctuations are assumed to be statistically homogeneous in the directions parallel to the TNTI, x_1 and x_3. Attention will be focused on u_2, because it is the velocity component directly involved in the definition of $\theta(k_1, k_3)$ and, as shown by Phillips [10], its variance in the irrotational flow region is simply twice that of the velocity variances parallel to the TNTI, $\langle u_1^2\rangle$ and $\langle u_3^2\rangle$. u_2 can be expressed as a Fourier integral along the x_1 and x_3 directions:

$$u_2(x_1,x_2,x_3) = \int_{-\infty}^{+\infty}\int_{-\infty}^{+\infty}\hat{u}_2(k_1,x_2,k_3)e^{i(k_1x_1+k_3x_3)}dk_1dk_3, \tag{2}$$

where $\hat{u}_2$ is the Fourier transform of u_2. The RDT solutions of Teixeira *et al.* (2012) for the velocity fluctuations in an irrotational velocity field outside a region of homogeneous and isotropic turbulence are similar to those of Carruthers and Hunt [12] when the non-turbulent region is not stratified. The Fourier component of u_2, for example, is given by

$$\hat{u}_2(k_1,x_2,k_3) = \frac{1}{2}\int_{-\infty}^{+\infty}\hat{u}_2^{(H)}(k_1,k_2,k_3)e^{-k_{13}x_2}dk_2, \tag{3}$$

where $k_{13} = (k_1^2 + k_3^2)^{1/2}$, k_2 is the wave number in the direction perpendicular to the TNTI, and $\hat{u}_2^{(H)}$ is the Fourier transform of the u_2 velocity component in the homogenous and isotropic turbulence existing to the other side of the TNTI. It is known that, by definition of isotropic turbulence

$$\left\langle\hat{u}_i^{(H)}(\mathbf{k})\hat{u}_j^{(H)}(\mathbf{k}')\right\rangle = \Phi_{ij}^{(H)}(\mathbf{k})\delta(\mathbf{k}-\mathbf{k}'), \quad i,j=1,2,3, \tag{4}$$

where $\Phi_{ij}^{(H)}$ is the three-dimensional wave-number spectrum of the isotropic turbulence velocity, $\mathbf{k} = (k_1, k_2, k_3)$, $\mathbf{k}' = (k_1', k_2', k_3')$, and δ is the Dirac delta function. If (2)–(4) are inserted into (1), this yields

$$\theta(k_1,k_3) = \frac{1}{4}\int_{-\infty}^{+\infty}\Phi_{22}^{(H)}(\mathbf{k})dk_2. \tag{5}$$

In isotropic turbulence, the 3D wave-number spectrum is related to the energy spectrum of the turbulence $E(k)$ in the following way:

$$\Phi_{ij}^{(H)}(\mathbf{k}) = \left(\delta_{ij} - \frac{k_ik_j}{k^2}\right)\frac{E(k)}{4\pi k^2}, \quad i,j=1,2,3, \tag{6}$$

where δ_{ij} is the Kronecker delta and $k = (k_1^2 + k_2^2 + k_3^2)$ is the wave-number magnitude. Using (6), (5) can be expressed as

$$\theta(k_1,k_3) = \frac{k_{13}^2}{8\pi}\int_0^{+\infty}\frac{E(k)}{k^4}dk_2, \tag{7}$$

where it was assumed that $E(k)$ is an even function of k_2 (which is justified, because it only depends on k). Using (2)–(6), it is also possible to show that the variance of the u_2 velocity component in the irrotational flow region is given by

$$\langle u_2^2\rangle = \frac{1}{16\pi}\int_{-\infty}^{+\infty}\int_{-\infty}^{+\infty}\int_{-\infty}^{+\infty}\frac{k_{13}^2}{k^4}E(k)e^{-2k_{13}x_2}dk_1dk_2dk_3. \tag{8}$$

Using (7), this can also be expressed in terms of $\theta(k_1, k_3)$ as

$$\langle u_2^2\rangle = \int_{-\infty}^{+\infty}\int_{-\infty}^{+\infty}\theta(k_1,k_3)e^{-2k_{13}x_2}dk_1dk_3, \tag{9}$$

which can also be written

$$\langle u_2^2\rangle = 2\pi\int_0^{+\infty}k_{13}\theta(k_{13})e^{-2k_{13}x_2}dk_{13}, \tag{10}$$

where in the integral polar coordinates, $k_1 = k_{13}\cos\lambda$ and $k_3 = k_{13}\sin\lambda$ have been introduced, and the integration along the azimuthal angle λ was carried out analytically. This result uses the fact that $\theta(k_1, k_3)$ is only a function of k_{13}, which can easily be inferred from (7).

Equation (10) clearly shows why at large distances from the TNTI (i.e., large x_2), only small values of the wave number k_{13} contribute to the velocity variance. Any wave numbers other than the smallest ones will lead to a small value of the exponential. With this in mind, it is possible to infer the behavior of the variance by studying the behavior of $\theta(k_{13})$ as defined by (7). That equation shows that, if the limit of the integral as $k_{13} \to 0$ is a nonzero constant, $\theta(k_{13})$ is proportional to k_{13}^2, as was assumed by Phillips [10] [see his

Eq. (20)]. This corresponds to a Batchelor spectrum, which at low wave numbers is $E(k) \sim k^4$, as was shown by Teixeira and da Silva [14], and will be confirmed and extended next.

Consider a generic form for the energy spectrum of the turbulence $E(k)$, such that this spectrum is asymptotically proportional to k^n at low wave numbers,

$$E(k) = k^n f(k), \tag{11}$$

where n is a non-negative integer number, and $f(k)$ is function that must tend to a nonzero constant as $k \to 0$. For the spectrum to be physically consistent, $f(k)$ must also decay to zero as $k \to \infty$ at an appropriate rate, such that the spectrum, when integrated over k, adds up to a finite energy. With these properties, it is clear that if $n \geqslant 4$, the integral of $E(k)/k^4$ in (7) as $k_{13} \to 0$, i.e., as $k \to k_2$, must converge to a nonzero constant. Hence, for all cases where $n \geqslant 4$ (which include the case of a Batchelor spectrum, $n = 4$), $\theta(k_{13})$ is proportional to k_{13}^2 for low k_{13}. Now, if this fact is used in (10), it must be concluded (by calculating the integral in that equation by parts multiple times) that $\langle u_2^2 \rangle \sim x_2^{-4}$. So, for any $n \geqslant 4$, the velocity variance always decays proportionally to x_2^{-4} for large x_2. The behavior of u_2^2 in other cases, namely, $n < 4$, depends on how the dependence of $\theta(k_{13})$ on k_{13} for low values of this variable differs from k_{13}^2.

For integer n, only the cases $n = 1, 2, 3$ need to be considered, since $n = 0$ would correspond to an energy spectrum where the integral length scale is not properly defined (see Eq. (4.15) of Teixeira and Belcher [30]). Each case needs to be treated separately. The case $n = 2$ was already addressed by Xavier *et al.* (2021) for a specific exponential form of $f(k)$, but will be repeated here under more general conditions. For treating the cases $n = 1, 2, 3$, it is useful to split the integral in (7) into two parts,

$$\int_0^{+\infty} \frac{E(k)}{k^4} dk_2 = \int_0^{k_0} k^{n-4} f(k) dk_2 + \int_{k_0}^{+\infty} k^{n-4} f(k) dk_2, \tag{12}$$

where (11) has been used, and $k_0 > 0$ is a wave number value below which $f(k)$ is constant to a good degree of approximation. The second integral in (12) always evaluates to a finite constant when $k_{13} \to 0$ for any value of n (provided $f(k)$ decays to zero sufficiently fast as $k \to \infty$) because the only reason for the integral not to converge could only come from the lower limit k_0, but since k_0 is positive, this never occurs. The first integral also evaluates to a constant when $k_{13} \to 0$ in the case $n \geqslant 4$ (hence the results presented above), but when $n < 4$ it diverges at $k_3 = 0$ when $k_{13} \to 0$, dominating the full integral on the left-hand side of (12), and thus changing the dependence of θ on k_{13}. For this effect to be perceived and evaluated correctly, the limit $k_{13} \to 0$ must be taken after the integral has been calculated.

Then the first integral on the right-hand side of (12) is

$$\int_0^{k_0} k^{n-4} f(k) dk_2 \approx f(k=0) \int_0^{k_0} k^{n-4} dk_2 = f(k=0) \int_0^{k_0} (k_{13}^2 + k_2^2)^{\frac{n-4}{2}} dk_2. \tag{13}$$

Consider first the case $n = 1$. Then,

$$\int_0^{k_0} (k_{13}^2 + k_2^2)^{\frac{n-4}{2}} dk_2 = \int_0^{k_0} (k_{13}^2 + k_2^2)^{-\frac{3}{2}} dk_2 = \frac{k_0}{k_{13}^2 (k_{13}^2 + k_0^2)^{1/2}}. \tag{14}$$

The limit of this expression as $k_{13} \to 0$ is k_{13}^{-2}. Therefore, when inserted in (7) this makes θ approach a constant (i.e., lose its dependence on k_{13}), so calculation of the integral in (10) yields a dependence of the velocity variance $\sim x_2^{-2}$. In the case $n = 2$ (treated by Xavier *et al.* [28]), the integral on the right-hand side of (13) becomes instead

$$\int_0^{k_0} (k_{13}^2 + k_2^2)^{\frac{n-4}{2}} dk_2 = \int_0^{k_0} (k_{13}^2 + k_2^2)^{-1} dk_2 = \frac{1}{k_{13}} \arctan\left(\frac{k_0}{k_{13}}\right), \tag{15}$$

which approaches $\pi/(2k_{13})$ when $k_{13} \to 0$. This makes θ become proportional to k_{13}, which from (10) implies that the velocity variance is proportional to x_2^{-3}. This is the result obtained by Xavier *et al.* [28] for a particular form of the turbulence energy spectrum where the function $f(k)$ in (11) is Gaussian.

Finally, in the case $n = 3$, the integral on the right-hand side of (13) becomes

$$\int_0^{k_0} (k_{13}^2 + k_2^2)^{\frac{n-4}{2}} dk_2 = \int_0^{k_0} (k_{13}^2 + k_2^2)^{-\frac{1}{2}} dk_2 = \ln\left[\frac{(k_{13}^2 + k_0^2)^{1/2} + k_0}{k_{13}}\right]. \tag{16}$$

In the limit $k_{13} \to 0$, this reduces to $\ln(2k_0/k_{13}) \sim -\ln(k_{13})$. This means that $\theta \propto -k_{13}^2 \ln(k_{13})$, and so it can be shown that in this case (10) determines the velocity variance to be proportional to $x_2^{-4} \ln(x_2)$ as $x_2 \to \infty$. This type of variation is intermediate between x_2^{-3} and x_2^{-4}, as would perhaps be expected intuitively.

A. Exact and asymptotic results for an exponential energy spectrum

All the preceding results have been derived, in general (and without a quantitative specification of the asymptotic behavior of $\langle u_2^2 \rangle$ apart from proportionality to a type of function of x_2), for a generic energy spectrum. To be more specific and confirm that these results are indeed valid for any energy spectrum, a number of examples will be presented next for the case of an exponential energy spectrum similar to those adopted by Teixeira and da Silva [14] and Xavier *et al.* [28]. Only the cases $n = 1, 2, 3, 4, 5, 6$ will be considered, since for higher values of n the behavior of the velocity variance is qualitatively similar, as noted in the preceding section. Recall that the case $n = 1$ corresponds to a situation where the Reynolds number is constant (inside the neighboring turbulent region) [27], whereas the cases $n = 5$, 6 (or bigger) can be used to represent an isotropic flow evolving with a constant integral scale [27]. The case $n = 3$ would represent another intermediate, physically valid, condition [26].

A preliminary point must be made about the specification of the energy spectrum. If an exponential form is used, the coefficients included in the spectrum are specific for each value of n chosen, and it is convenient to treat separately the cases with n even or odd. Hence, for odd $n = 2m + 1$ (where m is an integer),

$$E(k) = \alpha(q^2\lambda_\infty)(k\lambda_\infty)^{2m+1}\mathrm{e}^{-\beta(k\lambda_\infty)^2}, \tag{17}$$

where q is the root-mean-square (RMS) velocity in the homogeneous and isotropic turbulence, λ_∞ is the corresponding Taylor microscale, and the coefficients α and β must be defined as

$$\alpha = \frac{3}{2^{m+1}m!}\left(\frac{2m+2}{5}\right)^{m+1}, \quad \beta = \frac{m+1}{5}. \tag{18}$$

The equations in (18) ensure that the energy spectrum given by (17) satisfies the constraint of integrating to $3q^2/2$, and when multiplied by $2\nu k^2$ (where ν is the kinematic viscosity) integrating to ε_∞, the dissipation rate in the homogeneous and isotropic turbulence. To satisfy the same constraints, for even $n = 2m$, the energy spectrum is defined as

$$E(k) = \gamma(q^2\lambda_\infty)(k\lambda_\infty)^{2m}\mathrm{e}^{-\delta(k\lambda_\infty)^2}, \tag{19}$$

where

$$\gamma = \frac{3}{(2\pi)^{1/2}}\frac{2^m m!}{(2m)!}\left(\frac{2m+1}{5}\right)^{m+\frac{1}{2}}, \quad \delta = \frac{2m+1}{10}. \tag{20}$$

For the cases $m = 0, 1, 2$, i.e., $n = 1, 3, 5$, the values taken by α and β are

$$\alpha = \tfrac{3}{5}, \quad \beta = \tfrac{1}{5} \quad (n = 1), \tag{21}$$

$$\alpha = \tfrac{12}{25}, \quad \beta = \tfrac{2}{5} \quad (n = 3), \tag{22}$$

$$\alpha = \tfrac{324}{1000}, \quad \beta = \tfrac{3}{5} \quad (n = 5), \tag{23}$$

whereas for the cases $m = 1, 2, 3$, i.e., $n = 2, 4, 6$, the values taken by γ and δ are

$$\gamma = \frac{9}{5}\left(\frac{3}{10\pi}\right)^{1/2}, \quad \delta = \frac{3}{10} \quad (n = 2), \tag{24}$$

$$\gamma = \frac{1}{(2\pi)^{1/2}}, \quad \delta = \frac{1}{2} \quad (n = 4), \tag{25}$$

$$\gamma = \frac{343}{625}\left(\frac{7}{10\pi}\right)^{1/2}, \quad \delta = \frac{7}{10} \quad (n = 6). \tag{26}$$

Note that the cases $n = 4$ and $n = 2$ have been obtained previously by Teixeira and da Silva [14] and Xavier *et al.* [28], respectively.

It is now possible to calculate the velocity variance for all the cases introduced above. For this purpose, it is only necessary to insert the expression for the energy spectrum, corresponding either to Eq. (17) or Eq. (19), into the expression for the velocity variance, Eq. (8). When this is done, $\langle u_2^2(x_2)\rangle$ can only be evaluated numerically, in general, but due to the simplifications outlined above when $k_{13} \to 0$, it is possible to obtain the asymptotic limit of $\langle u_2^2\rangle$ for $x_2 \to \infty$ for all cases as closed analytical expressions. These expressions

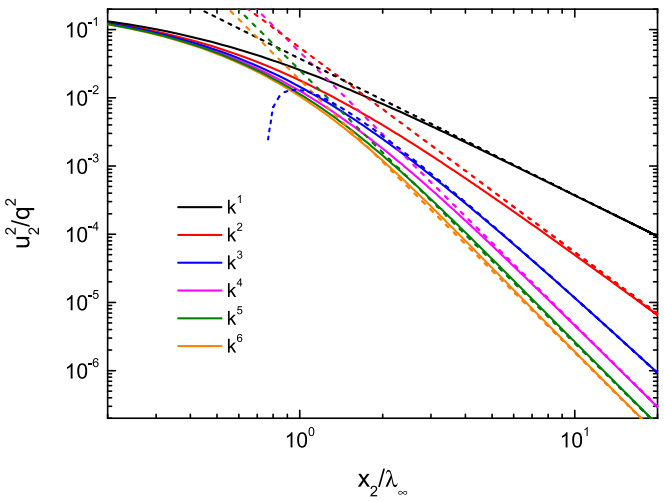

FIG. 1. Variance of the velocity perpendicular to the TNTI $\langle u_2^2\rangle$ in the irrotational flow region as a function of distance from the TNTI normalized by the Taylor microscale of the homogeneous and isotropic turbulence (x_2/λ_∞). Solid lines: results from Eq. (8) using an energy spectrum proportional to k^n at low wave numbers; dashed lines: asymptotic approximations from Eqs. (27)–(32). Black lines: $n = 1$, red lines: $n = 2$, blue lines: $n = 3$, magenta lines: $n = 4$, green lines: $n = 5$, orange lines: $n = 6$.

are the following:

$$\langle u_2^2\rangle \sim \frac{3q^2}{80(x_2/\lambda_\infty)^2} \quad (n = 1), \tag{27}$$

$$\langle u_2^2\rangle \sim \left(\frac{3\pi}{10}\right)^{1/2}\frac{9q^2}{160(x_2/\lambda_\infty)^3} \quad (n = 2), \tag{28}$$

$$\langle u_2^2\rangle \sim \frac{3q^2}{400(x_2/\lambda_\infty)^4}[6\ln(x_2/\lambda_\infty) + 3\gamma_E + 3\ln(40) - 11] \quad (n = 3), \tag{29}$$

$$\langle u_2^2\rangle \sim \frac{3q^2}{64(x_2/\lambda_\infty)^4} \quad (n = 4), \tag{30}$$

$$\langle u_2^2\rangle \sim \frac{81q^2}{3200(x_2/\lambda_\infty)^4} \quad (n = 5), \tag{31}$$

$$\langle u_2^2\rangle \sim \frac{147q^2}{8000(x_2/\lambda_\infty)^4} \quad (n = 6), \tag{32}$$

where γ_E is the Euler-Mascheroni constant, $\gamma_E \approx 0.577$. Note how the result for $m = 3$ has a more complicated analytical form because of the logarithmic dependence. For $n \geqslant 4$, it would be, in principle, possible to obtain a generic formula (depending on n) for the asymptotic behavior of $\langle u_2^2\rangle$ with x_2, but that is of limited interest, since the form of the dependence on x_2 does not change, and only the coefficient multiplying x_2^{-4} changes slightly.

Figure 1 shows $\langle u_2^2\rangle$ as a function of x_2 for $n = 1, 2, 3, 4, 5, 6$ from Eq. (8) (solid lines) and the asymptotic behavior of these expressions from (27)–(32) (dashed lines). Clearly, the asymptotes approximate the exact expressions very closely for $x_2/\lambda_\infty \geqslant 10$. The asymptote for $n = 3$ has a rather unusual behavior at its left end because of the presence of the logarithmic function in (29), as the logarithm of

x_2/λ_∞ does not follow a straight line when represented using logarithmic axes, and becomes negative when $x_2/\lambda_\infty < 1$.

III. DIRECT NUMERICAL SIMULATIONS

A total of five DNS of SFT were carried out in this paper. All simulations use the same code already employed and validated for a similar simulation in Ref. [28]. Each one of the simulations is done in two steps, comprising (i) an initial DNS of decaying homogeneous isotropic turbulence (DHIT) followed by (ii) a simulation of SFT, where a turbulent front is generated that spreads into the nonturbulent (irrotational) flow region in the absence of mean shear.

A. Numerical methods

The code used in the simulations is an in-house Navier-Stokes solver using pseudospectral methods (collocation method) for spatial discretization [31], and a three-step third-order explicit Runge-Kutta scheme for the temporal advancement [32]. The domain is a triple periodic cube with sides equal to 2π and the simulations are fully dealiased with the 2/3 rule, and employ $N_1 \times N_2 \times N_3$ collocation points in the x_1, x_2, and x_3 directions, respectively [28].

B. DNS of decaying free shear turbulent fronts

The five DNS carried out in this paper mainly differ in the details of the initial velocity field. This is obtained from a random number generator that creates a divergence-free velocity field with initial variance equal to $\langle u_1^2\rangle = \langle u_2^2\rangle = \langle u_3^2\rangle = 1$, and with a prescribed three-dimensional kinetic energy spectrum following,

$$E(k) \sim k^n e^{-2\left(\frac{k}{k_p}\right)^2}, \tag{33}$$

where k_p is the peak wave number and n is the slope in the low wave number (infrared) region [33]. We designate by k^1 to k^5 the five simulations carried out in this paper, where the parameter n was set as $n = 1$ to $n = 5$, respectively. In all cases, the kinematic viscosity was set to $\nu = 3 \times 10^{-4}$, while the peak wave number was $k_p = 30$ as in Ref. [28]. The cases $n = 2$ and $n = 4$ correspond to the so-called Saffman turbulence [23] and Batchelor turbulence [34], respectively, and were already discussed in Ref. [28]. A total of $N_1 \times N_2 \times N_3 = 512 \times 512 \times 512$ collocation points was used for all the simulations, except for the case $K5$ where $N_1 \times N_2 \times N_3 = 1024 \times 1024 \times 1024$ points have been used.

Similarly to Ishida *et al.* [33] and Xavier *et al.* [28], the Reynolds number is defined as $\mathrm{Re}_{k_p} = \langle u^2\rangle^{1/2}/(k_p\nu)$, and the time is normalized by the initial integral timescale (or turnover timescale) $T_{k_p} = 1/(\langle u^2\rangle^{1/2} k_p)$ that is $\tau = t/T_{kp}$. The initial Reynolds number for all the simulations is equal to $\mathrm{Re}_{k_p} = 125$, and the kinetic energy spectrum peaks at $k_p = 30$, which again are equal to the simulations of Ishida *et al.* [33] and Xavier *et al.* [28]. As discussed in these works, the values of Re_{k_p} and k_p are set to preserve the slope of the kinetic energy spectrum at low wave numbers during the kinetic energy decay phase and to obtain the theoretical kinetic energy decay rates in DNS of DHIT ($\mathrm{Re}_{k_p} > 100$ and $k_p > 20$ [28,33]). Finally, note that the ratio of the maximum effective wave number $k_{\max}$ and the peak wave number is equal to $k_{\max}/k_p = 12$, which maximizes the Reynolds number Re_{k_p}, while keeping an appropriate resolution.

Starting with these initial conditions, each DHIT simulation (k^1 to k^5) undergoes the typical evolution described in many previous works, i.e., the enstrophy increases initially with time as the kinetic energy spectrum spreads into higher wake numbers $k > k_p$, until it attains a maximum (τ_ω: enstrophy peak), which is then followed by a slow decay (e.g., Refs. [28,33]). Eventually, after the enstrophy peak has been attained, the velocity variance for the cases k^4 and k^2 recovers the power laws $\langle u^2\rangle \sim \tau^{-10/7}$ and $\langle u^2\rangle \sim \tau^{-6/5}$ predicted by the classical theory [11], as described in the similar simulations from Ref. [28].

Figure 2 shows the initial kinetic energy spectrum of several simulations prior to the generation of the SFT simulations. The difficulty of achieving the desired slopes for the infrared region of the kinetic energy spectra in DNS is well-known [33], however, the present spectra are reasonably close to the target values. For the cases $k = 1, 2, 3, 4, 5$, the low wave-number slopes are equal to $n \approx 1.0, 1.9, 2.8, 3.7, 5.2$, respectively, considering the wave numbers between 3 and 5, where the slopes were obtained using a linear regression estimate. In any case, as can be observed, the infrared region of the kinetic energy spectra approximately follow the prescribed power laws.

C. Direct numerical simulations of shear-free turbulence

The five DNS of SFT corresponding to simulations k^1 to k^5 are then started from these fields (for a time instant τ_{SFT} after the enstrophy peak $\tau_{\mathrm{SFT}} > \tau_\omega$), following the procedure described in Refs. [35–37]. By using a convolution function (hyperbolic tangent), the flow field is separated into two regions, a central region where the velocity from the previous DHIT simulation is kept constant ($H/2 \leqslant x_2 \leqslant H/2$) and another region ($x_2 < -H/2 \ \wedge \ x_2 > H/2$) where the velocity field field is set to zero (H is a parameter defining the width of the initial turbulent region). The resulting flow field will then evolve for a few time steps and the initial isotropic turbulence flow region will slowly spread into the irrotational (quiescent) region, in the absence of mean shear. As in Ref. [28], it was checked that the value of H chosen does not affect the large scales of motion (as observed in the shape of the kinetic energy spectrum in the infrared region) and that the size of the nonturbulent region ($2\pi - 2H$) is sufficient to ensure that it is not affected by the (periodic) boundary conditions.

As in Zecchetto and da Silva [38], Xavier *et al.* [28], and many other works, the identification of the TNTI layer was done using the *volume method* described in detail in Taveira *et al.* [39], which allows one to identify the IB, which is the outermost layer of the TNTI. The procedure analyzes the variation of the vorticity magnitude ω with the volume of the turbulent flow region and allows one to obtain the vorticity magnitude threshold ω_{th} that identifies the IB.

Figure 3 shows a zoom of the flow region near the TNTI for the simulations k^2 and k^4, at approximately the same instant ($\tau \approx 30$) for the two cases, where the TNTI can be appreciated. In these simulations, the TNTI is very sharp and the turbulent region (T) contains a large number of

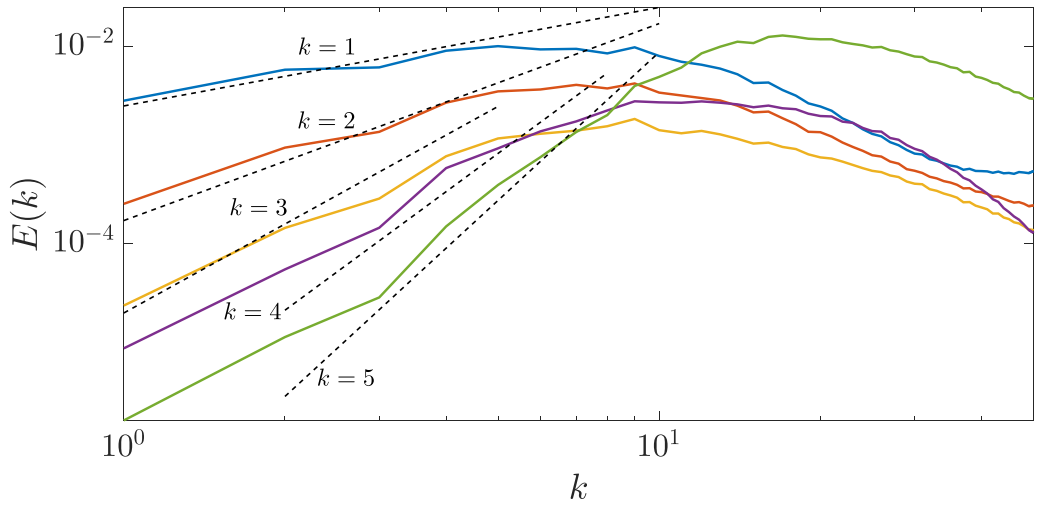

FIG. 2. Initial kinetic energy spectrum for the five DNS of DHIT used in the present paper. k^2 and k^4 correspond to the cases where the parameter n in Eq. (33) was set to 2 and 4, respectively, and were recently addressed by Ref. [28].

large-scale eddies, unconstrained by the presence of the boundary conditions.

D. Verification of the generalized asymptotic laws for the potential velocity fluctuations in DNS of SFT

To compare the theoretical results derived in Sec. II A with the results obtained from DNS Fig. 4 shows conditional profiles of normal velocity variance in the NT region $\langle u_2^2\rangle_I$ (see, e.g., Zecchetto and da Silva [38]), as a function of the magnitude of the distance from the irrotational boundary $\langle x_2\rangle_I$,for all the SFT simulations carried out in this work (k^1 to k^5). The results are compared with power laws defined by

$$\langle u_2^2\rangle_I \sim \langle x_2\rangle_I^{-p}, \tag{34}$$

as predicted by Eqs. (27)–(32) for $n = 1$ to $n = 6$, respectively, where the kinetic energy spectrum is described by a power law $E(k) \sim k^n$ in the infrared region. Notice that power laws of the type described by Eq. (34) are predicted for all these cases except for $n = 3$, where the decay law is less simple, but even this case is barely distinguishable in practice from the case $n = 4$ as discussed above (see Fig. 1).

According to the equations derived in Sec. II A, the correspondence between the power laws of the kinetic energy spectrum $E(k) \sim k^n$ and the power laws of the velocity variance $\langle u_2^2\rangle_I \sim \langle x_2\rangle_I^{-p}$ in the nonturbulent region go as follows:

$$n = 1 \rightarrow p = 2,$$
$$n = 2 \rightarrow p = 3,$$
$$n = 3 \rightarrow p \approx 4,$$
$$n = 4, 5, 6 \rightarrow p = 4.$$

It is clear that the curves from the DNS data closely follow the predicted power laws for a sufficiently large distance from the

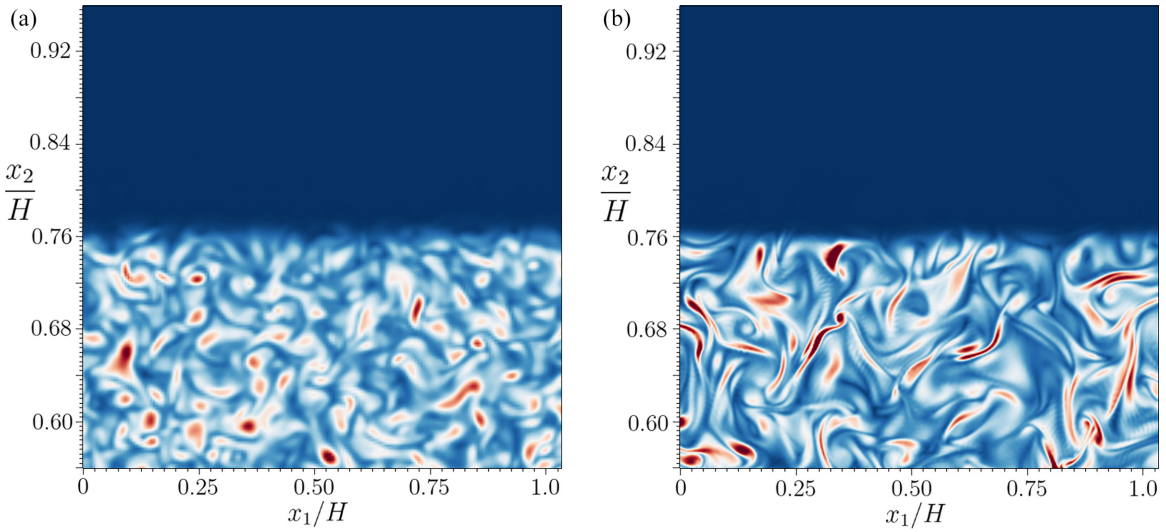

FIG. 3. Zoom of the enstrophy contours in the (x_1, x_2) plane near the TNTI for the (a) k^2 and (b) k^4 simulations at similar time instants (k^4 for $\tau = 31.43$ and k^2 for $\tau = 33.78$). Notice that the figures show only half of the turbulent region $H/2$).

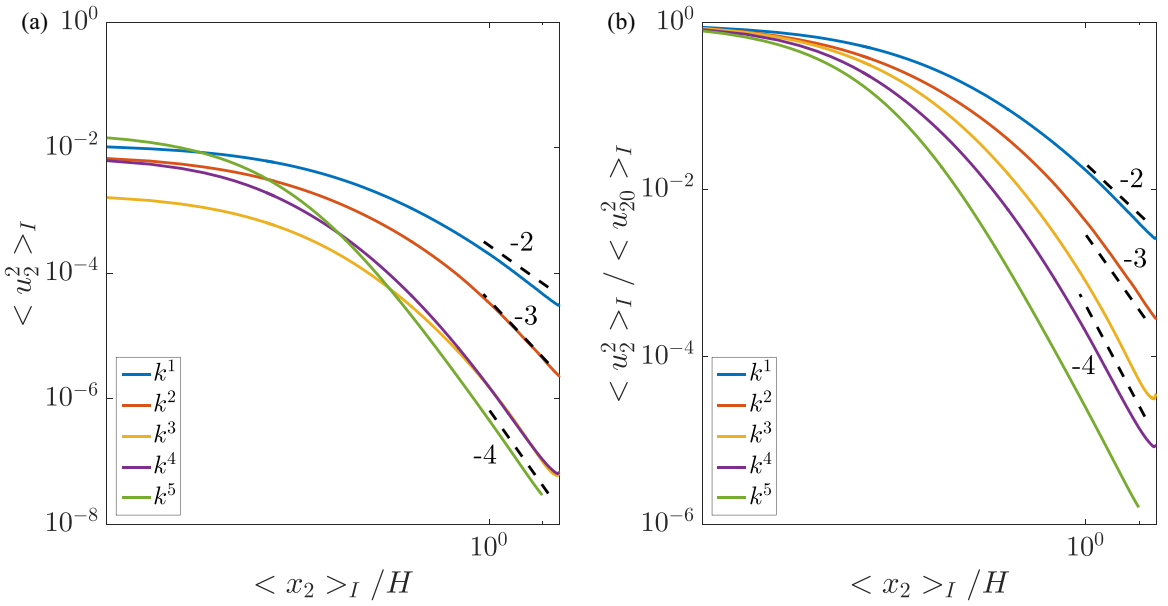

FIG. 4. (a) Conditional profiles of normal velocity variance $\langle u_2^2 \rangle_I$ in the NT region for all the SFT simulations (k^1 to k^5): (b) same as (a) but normalized by the initial normal velocity variance at the IB position. The profiles exhibit regions with power laws of $\langle u_2^2 \rangle_I \sim \langle x_2 \rangle_I^{-4}$, $\langle u_2^2 \rangle_I \sim \langle x_2 \rangle_I^{-3}$, and $\langle u_2^2 \rangle_I \sim \langle x_2 \rangle_I^{-2}$.

IB position. The small change observed for the DNS curves at the end of the lines merely indicate minor possible effects from the presence of the periodic boundary conditions. Even more compelling evidence of the power laws described in the theoretical expressions outlined above is given in Fig. 5, which shows the values of the power exponents p obtained from the asymptotic approximations computed in practice as

$$-p = \frac{\langle x_2 \rangle_I}{\langle u_2^2 \rangle_I} \frac{d\langle u_2^2 \rangle_I}{d\langle x_2 \rangle_I}. \tag{35}$$

The value of the exponents $-p$ are not only monotonous with n, but follow closely the predicted theoretical results for distances from the IB of $y/H \gtrsim 1$, thus demonstrating the accuracy of the predictions.

Finally, Fig. 6 shows the same profiles of normal velocity variance displayed in Fig. 4, but using classical statistics, i.e., $\langle u_2^2 \rangle_z$, where the averages are obtained by averaging the velocity field in the spanwise (z) direction. Similarly to Figs. 4(a) and 4(b), the profiles show regions with power laws predicted by the theoretical relations, although with a slightly stronger effect of the boundary conditions as observed by the end of the curves. The fact that these power laws are also observed in these classical statistics reinforces the relevance of the present theoretical results.

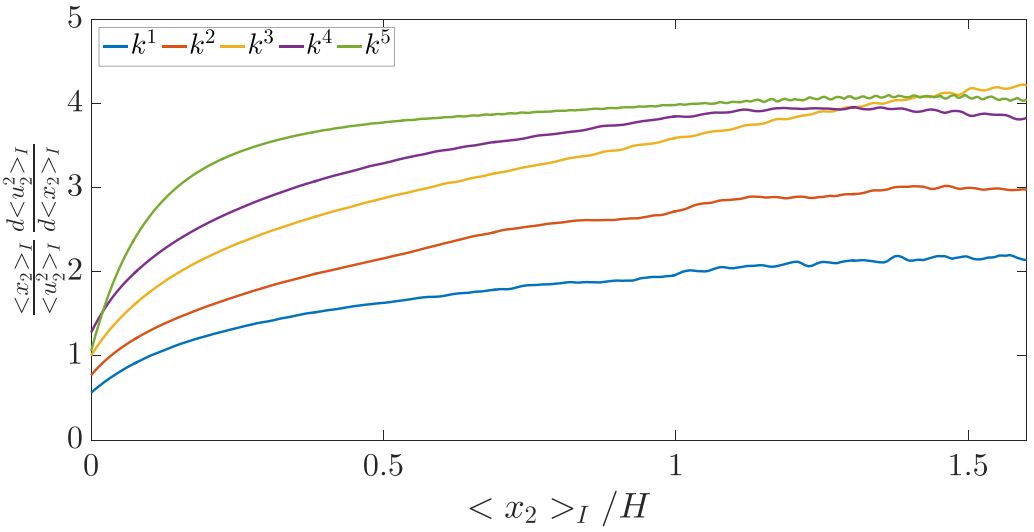

FIG. 5. Variation of the velocity variance decay exponent m defined in Eq. (35) for all the SFT simulations (k^1 to k^5). The colors are the same as in Fig. 4.

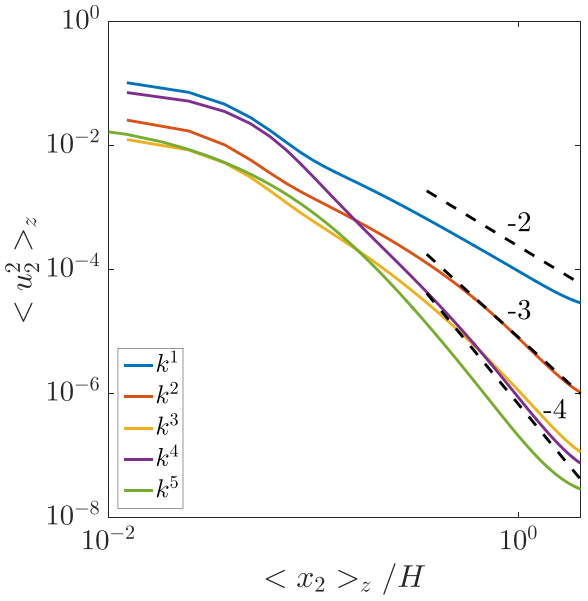

FIG. 6. Profiles of normal velocity variance $\langle u_2^2 \rangle_z$, in the NT region for all the SFT simulations (k^1 to k^5), where the averages are obtained by averaging the velocity field in the spanwise (z) direction. The profiles exhibit regions with power laws of $\langle u_2^2 \rangle_z \sim \langle x_2 \rangle_z^{-4}$, $\langle u_2^2 \rangle_z \sim \langle x_2 \rangle_z^{-3}$, and $\langle u_2^2 \rangle_z \sim \langle x_2 \rangle_z^{-2}$.

IV. CONCLUSIONS

Regions of potential velocity fluctuations exist at the nonturbulent (or irrotational) flow region bordering turbulent jets, wakes, mixing layers, and boundary layers, caused by the nonlocal influence of the large-scale eddy structures in the neighboring turbulent region. For large distances x_2 from the turbulent region, typically $x_2/L > 1$, where L is the longitudinal integral scale of motion inside the turbulent core region, the potential velocity fluctuations decay with a power law, whose exponent is imposed by the shape of the kinetic energy spectrum in the infrared region. In particular, it has been shown using analytical models that for power spectra of types $E(k) \sim k^4$ (Batchelor spectrum) and $E(k) \sim k^2$ (Saffman spectrum), the variance of the potential velocity fluctuations vary as $\langle u_i^2 \rangle \sim x_2^{-4}$ and $\langle u_i^2 \rangle \sim x_2^{-3}$, respectively [10,28]. These theoretical results have been recovered in experimental data [15–22] and also in recent DNSs [9,14,28].

In the present paper, these theoretical results were extended by using rapid-distortion theory to address the more general case of spectra with the form $E(k) \sim k^n$, where n is an integer, since several authors have reported the existence of spectra in the form $E(k) \sim k^n$, where n is different from $n = 4$ or $n = 2$ [24–27]. The theoretical results recover the classical solutions for $n = 4$ and $n = 2$, and lead to unique results for other cases. Particular cases include the laws $\langle u_i^2 \rangle \sim x_2^{-2}$ and $\langle u_i^2 \rangle \sim x_2^{-4}$, corresponding to $n = 1$ and $n \geqslant 5$, respectively, together with the case $n = 3$, for which $\langle u_i^2 \rangle \sim x_2^{-4} \ln(x_2)$.

Finally, five DNSs were carried out to assess the theoretical results using simulations of shear free turbulence where turbulent fronts spread into regions of irrotational flow in the absence of mean shear. The five simulations were designed to reproduce TNTIs where the kinetic energy spectrum in the infrared region follows a power law of the form $E(k) \sim k^n$, with the cases $n = 1,\ 2,\ 3,\ 4$, and $n = 5$.

For each one of the five DNSs, the velocity variance in the NT region was computed through both classical and conditional statistics (in relation to the distance from the IB), and show that the theoretical results are recovered in the DNS of shear-free turbulence.

We end by recalling that, as discussed in Xavier *et al.* [28] and references therein, these theoretical results are robust and insensitive to particular changes in the form of the kinetic energy spectrum for large wave numbers, as well as to the magnitude of the Reynolds number. Again, as argued in Xavier *et al.* [28], these results should also be valid for TNTIs existing in other flow types, including the effects of mean shear, such as jets or wakes, provided the kinetic energy spectra in the turbulence region exhibits a power law of the type $E(k) \sim k^n$, where n is an integer.

ACKNOWLEDGMENTS

C.B.d.S. acknowledges Fundação para a Ciência e Tecnologia (FCT) through IDMEC, under LAETA, Project No. UIDB/50022/2020 and scholarship 10.54499/SFRH/BD/144291/2019. The authors acknowledge Minho Advanced Computing Center for providing HPC computing and consulting resources that have contributed to the research results reported within this paper [40]. The authors acknowledge the Laboratory for Advanced Computing at University of Coimbra for providing HPC, computing, and consulting resources [41].

[1] S. B. Pope, *Turbulent Flows* (Cambridge University Press, 2000).

[2] D. K. Bisset, J. C. R. Hunt, and M. M. Rogers, The turbulent/non-turbulent interface bounding a far wake, J. Fluid Mech. **451**, 383 (2002).

[3] J. Westerweel, C. Fukushima, J. M. Pedersen, and J. C. R. Hunt, Momentum and scalar transport at the turbulent/non-turbulent interface of a jet, J. Fluid Mech. **631**, 199 (2009).

[4] C. B. da Silva, J. C. R. Hunt, I. Eames, and J. Westerweel, Interfacial layers between regions of different turbulent intensity, Annu. Rev. Fluid Mech. **46**, 567 (2014).

[5] C. B. da Silva, R. J. N. dos Reis, and J. C. F. Pereira, The intense vorticity structures near the turbulent/non-turbulent interface a jet, J. Fluid Mech. **685**, 165 (2011).

[6] T. Watanabe, R. Jaulino, R. Taveira, C. B. da Silva, K. Nagata, and Y. Sakai, Role of an isolated eddy near the turbulent/non-turbulent interface layer, Phys. Rev. Fluids **2**, 094607 (2017).

[7] M. M. Neamtu-Halic, D. Krug, G. Haller, and M. Holzner, Lagrangian coherent structures and entrainment near the turbulent/non-turbulent interface of a gravity current, J. Fluid Mech. **877**, 824 (2019).
[8] J. Westerweel, C. Fukushima, J. M. Pedersen, and J. C. R. Hunt, Mechanics of the turbulent-nonturbulent interface of a jet, Phys. Rev. Lett. **95**, 174501 (2005).
[9] R. R. Taveira and C. B. da Silva, Kinetic energy budgets near the turbulent/nonturbulent interface in jets, Phys. Fluids **25**, 015114 (2013).
[10] O. M. Phillips, The irrotational motion outside a free turbulent boundary, Proc. Camb. Phil. Soc. **51**, 220 (1955).
[11] P. A. Davidson, *Turbulence, an Introduction for Scientists and Engineers* (Oxford University Press, 2004).
[12] D. J. Carruthers and J. C. R. Hunt, Velocity fluctuations near an interface between a turbulent region and a stably stratified layer, J. Fluid Mech. **165**, 475 (1986).
[13] P. Sagaut and C. Cambon, *Homogeneous Turbulence Dynamics*, 2nd ed. (Springer, 2018).
[14] M. A. C. Teixeira and C. B. da Silva, Turbulence dynamics near a turbulent/non-turbulent interface, J. Fluid Mech. **695**, 257 (2012).
[15] R. M. Thomas, Conditional sampling and other measurements in a plane turbulent wake, J. Fluid Mech. **57**, 549 (1973).
[16] G. Fabris, Conditional sampling study of the turbulent wake of a cylinder. Part 1, J. Fluid Mech. **94**, 673 (1979).
[17] R. A. Antonia, D. A. Shah, and L. W. B. Browne, The organized motion outside a turbulent wake, Phys. Fluids **30**, 2040 (1987).
[18] I. Wygnanski and H. E. Fiedler, The two-dimensional mixing region, J. Fluid Mech. **41**, 327 (1970).
[19] L. J. S. Bradbury, The structure of a self-preserving turbulent plane jet, J. Fluid Mech. **23**, 31 (1965).
[20] M. Sunyach and J. Mathieu, Zone de melange d'un jet plan fluctuations induites dans le cone a potentiel-intermittence,Int. J. Heat Mass Transf. **12**, 1679 (1969).
[21] P. Bradshaw, Irrotational fluctuations near a turbulent boundary layer, J. Fluid Mech. **27**, 209 (1967).
[22] L. S. G. Kovasznay, V. Kibens, and R. F. Blackwelder, Large-scale motion in the intermittent region of a turbulent boundary layer, J. Fluid Mech. **41**, 283 (1970).
[23] P. G. Saffman, The large-scale structure of homogeneous turbulence, J. Fluid Mech. **27**, 581 (1967).
[24] G. Birkhoff, Fourier synthesis of homogeneous turbulence, Commun. Pure Appl. Math. **7**, 19 (1954).
[25] G. L. Eyink and D. J. Thomson, Free decay of turbulence and breakdown of self-similarity, Phys. Fluids **12**, 477 (2000).
[26] J. C. Vassilicos, An infinity of possible invariants for decaying homogeneous turbulence, Phys. Lett. A **375**, 1010 (2011).
[27] M. Oberlack and A. Zieleniewicz, Statistical symmetries and its impact on new decay modes and integral invariants of decaying turbulence, J. Turbul. **14**, 4 (2013).
[28] R. P. Xavier, M. A. C. Teixeira, and C. B. da Silva, Asymptotic scaling laws for the irrotational motions bordering a turbulent region, J. Fluid Mech. **918**, A3 (2021).
[29] J. C. R. Hunt and J. M. R. Graham, Free-stream turbulence near plane boundaries, J. Fluid Mech. **84**, 209 (1978).
[30] M. A. C. Teixeira and S. E. Belcher, Dissipation of shear-free turbulence near boundaries, J. Fluid Mech. **422**, 167 (2000).
[31] C. Canuto, M. Y. Hussaini, A. Quarteroni, and T. A. Zang, *Spectral Methods in Fluid Dynamics* (Springer-Verlag, 1987).
[32] J. H. Williamson, Low-storage Runge-Kutta schemes, J. Comput. Phys. **35**, 48 (1980).
[33] T. Ishida, P. A. Davidson, and Y. Kaneda, On the decay of isotropic turbulence, J. Fluid Mech. **564**, 455 (2006).
[34] G. K. Batchelor, *The Theory of Homogeneous Turbulence* (Cambridge University Press, 1953).
[35] B. Perot and P. Moin, Shear-free turbulent boundary layers. Part 1. Physical insights into near-wall turbulence, J. Fluid Mech. **295**, 199 (1995).
[36] A. Cimarelli, G. Cocconi, B. Frohnapfel, and E. De Angelis, Spectral enstrophy budget in a shear-less flow with turbulent/non-turbulent interface, Phys. Fluids **27**, 125106 (2015).
[37] T. S. Silva, M. Zecchetto, and C. B. da Silva, The scaling of the turbulent/non-turbulent interface at high Reynolds numbers, J. Fluid Mech. **843**, 156 (2018).
[38] M. Zecchetto and C. B. da Silva, Universality of small-scale motions within the turbulent/non-turbulent interface layer, J. Fluid Mech. **916**, A9 (2021).
[39] R. R. Taveira, J. S. Diogo, D. C. Lopes, and C. B. da Silva, Lagrangian statistics across the turbulent-nonturbulent interface in a turbulent plane jet, Phys. Rev. E **88**, 043001 (2013).
[40] https://macc.fccn.pt.
[41] http://www.lca.uc.pt.